Implied models approach for turbulence model form physics-based uncertainty quantification

Kerry S. Klemmer ⬡* and Michael E. Mueller
*Department of Mechanical and Aerospace Engineering, Princeton University, Princeton,
New Jersey 08544, USA*

Model form uncertainty arises from physical assumptions made in constructing models either to model physical processes that are not well understood or to reduce the physical complexity. Understanding these uncertainties is important for both quantifying prediction uncertainty and unraveling the source and nature of model errors. Physics-based uncertainty quantification utilizes inherent physical model assumptions to estimate and ascertain the sources of model form uncertainty or error. Compared to data-based approaches, physics-based approaches can be extrapolated beyond available data and go beyond strictly uncertainty estimation. In this work, an implied models approach is developed where the transport equation for the model error is derived by taking the difference between the exact transport equation for a quantity of interest and the transport equation implied by a particular model form. The implied models approach is then specifically applied to the modeling of the Reynolds stresses by the Boussinesq eddy viscosity model. Budgets of the model error transport are analyzed to better understand the sources of error in two-equation Reynolds-averaged Navier-Stokes models focusing on the relative contributions from the Boussinesq hypothesis and the specific form of the eddy viscosity in turbulent channel flow at various friction Reynolds numbers. The results indicate that the errors are largely due to the misalignment of the mean strain rate tensor and the Reynolds stress tensor as well as the high degree of anisotropy near the wall, with errors in the shear component being dominant. An exploration of the k-ε and k-ω models reveals that both models benefit from error cancellation. In particular, the improved results of the k-ω model over the k-ε model are shown to be the direct result of this error cancellation. An exploration of the effect of friction Reynolds number on the error budgets reveals that the errors saturate with increasing Reynolds number owing to the relative decrease of anisotropy.

I. INTRODUCTION

Reynolds-averaged Navier-Stokes (RANS) models and large-eddy simulation (LES) are widely used due to their relatively cheap computational cost compared to direct numerical simulation (DNS). However, the accuracy and fidelity of RANS and LES closure models are known to be extremely susceptible to both parametric and model form uncertainty. The parametric uncertainty in these models has been widely studied and deals with the uncertainty associated with the optimal choice of the model coefficients. The model form uncertainty present in RANS and LES closure models arises from the assumptions inherent in these models. Understanding the sources of model form uncertainty or error present in these models is paramount to the interpretation of the model outputs and the development of more accurate models.

---

*kklemmer@princeton.edu

Data-driven techniques have long been employed to quantify uncertainty in turbulence models. This has been achieved through both parametric uncertainty and, more recently, model form uncertainty quantification methods. Parametric uncertainty techniques treat the turbulence model parameters as random variables and propagate this uncertainty through the model, ultimately obtaining a probability density function for the quantity of interest (QOI). These methods only capture the uncertainty associated with the parameters, giving the user the optimal value of the model parameters for a given flow. This means that the model form uncertainty is not quantified or is embedded into the parametric uncertainty and so is not separately or well understood in this approach. Examples of this as applied to turbulence modeling can be found in work from Meldi *et al.* [1]. In that work, the authors studied the parametric uncertainty in two different models for the turbulent energy spectrum by introducing stochasticity into the free model parameters and using general polynomial chaos to propagate the uncertainty. In doing so, they look at the effect of these free model parameters on the resulting energy spectrum and subsequently the Smagorinsky model constant.

Model form uncertainty techniques have become increasingly more prevalent. Some of these leverage parametric uncertainty quantification (UQ) methods by incorporating an additional uncertainty parameter meant to quantify the model inadequacy or discrepancy. This has been done in the work from Edeling *et al.* [2] and Oliver and Moser [3], both of which use Bayesian estimation. In the former, parametric uncertainty as well as model inadequacy, through a multiplicative term, is quantified for the k-ε turbulence model. In the latter, various model inadequacy formulations are explored (multiplicative and additive through both the mean velocity and Reynolds stresses) and applied to multiple RANS models.

Other model form UQ approaches have specifically focused on introducing machine learning algorithms in aiding in the turbulence closure problem. These data-driven techniques use high-fidelity data from DNS or experiments to aid in closure of and estimation of the uncertainty in the turbulence model [4,5]. Generally, these works build off of existing UQ methodologies, such as Bayesian estimation, and introduce machine learning techniques, such as Gaussian process regression [4] or neural networks [4,5], in order to learn the functional form of the model discrepancy or inadequacy. These machine learning techniques have the advantage of being able to achieve a more complex model discrepancy but are ultimately still physics blind, save for the inclusion of data. It is important to note that these data-driven methods are limited by the availability of high-fidelity data, which in many cases is limited by computational cost or complexity, and the resulting model form uncertainties are unlikely to be extrapolatable much beyond the available data.

More recent work from Iaccarino and co-workers [6–8] has attempted to inject additional physics into model form uncertainty for RANS models. In all of these works, a physics-motivated approach is taken in which the anisotropic Reynolds stress tensor a_{ij} is decomposed into its eigenvalues and eigenvectors, and perturbations are then introduced into the eigenvalues in order to provide error bounds on the base RANS model. The decomposition of a_{ij} results in a direct representation of the magnitude, shape, and orientation of the Reynolds stresses via the turbulent kinetic energy, eigenvalues, and eigenvectors of the anisotropy tensor, respectively. In this way, perturbations can be introduced into these three different aspects of the Reynolds stresses and the uncertainty can be propagated to the QOIs, such as the mean velocity. Ultimately, this method uses perturbations towards the limiting states of the realizable Reynolds stresses as error bounds and in doing so they are able to capture the behavior of flows that were previously indescribable using linear eddy viscosity models for RANS closure, such as separated flows [8]. These approaches have been further extended by Gorlé and co-workers to modeling the scalar flux vector [9] and the pressure scrambling term in the scalar flux transport equation [10]. Additionally, this perturbation methodology has been coupled with machine learning techniques in order to learn the appropriate perturbations necessary to capture the physically correct flow [11,12].

The aforementioned works utilize methodologies that are able to characterize the uncertainty in RANS closure models through physically motivated perturbations to the structure of the anisotropic Reynolds stress tensor. In this way, this perturbation framework informs the user how to introduce

perturbations but not necessarily why these perturbations are needed. As such, the source of the model error, as in why the model fails to capture the correct physical behavior, is still unknown. In other words, this approach essentially highlights the shortcomings of the turbulence models but does not necessarily indicate the *root cause* of such errors. The cause, in many cases, is the inadequacy of the model assumptions, simplifications that are not necessarily applicable in all conditions, and the failure of inadequacy of these assumptions can only be assessed using fully physics-based UQ approaches. In some cases, these assumptions are easily identifiable and can be leveraged to provide estimates of model form uncertainty as in the work of Klemmer and Mueller [13]. In that work, a methodology was developed for assessing the uncertainty associated with a specific model assumption by a hierarchical UQ approach. In that approach, a hierarchy of models was identified and then the explicit assumptions were used to estimate the error between the different models in the hierarchy. While they looked at turbulent combustion models, the physics-based nature of their work is applicable to turbulence models as well. The present work builds upon this idea of utilizing the physical assumptions, the difference being that the explicit nature of the assumptions, which is not always known, is not the driving force behind the formulation. Instead, the present framework uses the implicit knowledge of the model assumptions embedded within the fundamental governing equations to characterize the sources of the model form uncertainty. In doing so, this framework provides insight regarding the reasons and conditions under which model assumptions are wrong.

In this work, a physics-based UQ methodology is developed and applied to two-equation RANS turbulence models in order to understand the model assumptions that contribute to model inadequacy or error. In the approach, the individual model assumptions are isolated through the derivation of a transport equation for the model error *implied* by the model. The general implied models approach is outlined in Sec. II, and this approach is then applied to RANS turbulence models in Sec. III. The results are presented in Sec. IV, where in Secs. IV A–IV C the implied models approach is applied to an incompressible turbulent channel flow at $\mathrm{Re}_\tau = 180$ and then in Sec. IV D extended to higher Re_τ.

II. IMPLIED MODELS APPROACH

Consider a quantity $\mathcal{R}$ to be modeled by $\mathcal{M}$. The difference between them is the model error e,

$$e = \mathcal{R} - \mathcal{M}. \tag{1}$$

The quantity $\mathcal{R}$ has an exact transport equation. Likewise, an analogous transport equation implied by the model $\mathcal{M}$ can be derived. The difference between these transport equations is the model error transport equation

$$\frac{De}{Dt} = \frac{D\mathcal{R}}{Dt} - \frac{D\mathcal{M}}{Dt}. \tag{2}$$

While this approach requires the existence of transport equations for $\mathcal{R}$ and $\mathcal{M}$, the result provides insightful information that would otherwise not be accessible with Eq. (1) alone. A transport equation for the error allows for a dynamical view of the processes that produce, transport, redistribute, and dissipate the model error, while the error itself only provides a static picture of the model error with no information as to its sources or transport mechanisms. As such, when available, a model error transport equation is a powerful and insightful tool that provides an enhanced understanding as well as specific identification of the model assumptions, through analysis of the budget of the model error transport equations, that contribute most to the model error.

III. APPLICATION TO RANS TURBULENCE MODELING

In turbulence, a transport equation can be derived for almost any physical quantity. This fact is exploited in the implied models approach such that a transport equation is derived for the error from the transport equations for the true physical quantity and the model. In the present work, the

anisotropic Reynolds stress tensor a_{ij} will be considered as the true physical quantity

$$\mathcal{R}_{ij} = a_{ij} = \overline{u_i' u_j'} - \tfrac{2}{3} k \delta_{ij}, \tag{3}$$

where $\overline{u_i' u_j'}$ is the Reynolds stress tensor and $k = \tfrac{1}{2} \overline{u_i' u_i'}$ is the turbulent kinetic energy. The anisotropic Reynolds stress tensor is modeled with the Boussinesq eddy viscosity model

$$\mathcal{M}_{ij} = -2 \nu_T S_{ij}, \tag{4}$$

where ν_T is the eddy viscosity and S_{ij} is the mean strain rate tensor. Substituting Eqs. (3) and (4) into Eqs. (1) and (2) yields

$$e_{ij} = a_{ij} + 2 \nu_T S_{ij} \tag{5}$$

and

$$\frac{\overline{D} e_{ij}}{Dt} = \frac{\overline{D} a_{ij}}{Dt} + 2 \nu_T \frac{\overline{D} S_{ij}}{Dt} + 2 S_{ij} \frac{\overline{D} \nu_T}{Dt}, \tag{6}$$

where $\frac{\overline{D}}{Dt}$ is the material derivative with convection by the mean velocity U_k. In order to obtain a transport equation for the model error e_{ij}, a transport equation for each of the three terms in Eq. (6) needs to be specified. For the Reynolds stress and mean strain rate tensors, these are straightforward. For an incompressible flow with constant viscosity, the transport equation for the anisotropic Reynolds stress tensor is given by

$$
\begin{aligned}
\frac{\overline{D} a_{ij}}{Dt} = & -\overline{u_i' u_k'} \frac{\partial U_j}{\partial x_k} - \overline{u_j' u_k'} \frac{\partial U_i}{\partial x_k} + \frac{2}{3} \overline{u_k' u_\ell'} \frac{\partial U_k}{\partial x_\ell} \delta_{ij} \\
& - \frac{\partial}{\partial x_k} \left(\overline{u_i' u_j' u_k'} - \frac{2}{3} \overline{k u_k'} \delta_{ij} - \nu \frac{\partial \overline{u_i' u_j'}}{\partial x_k} + \frac{2\nu}{3} \frac{\partial \overline{k}}{\partial x_k} \delta_{ij} \right) \\
& - \frac{1}{\rho} \left\langle u_i' \frac{\partial p'}{\partial x_j} + u_j' \frac{\partial p'}{\partial x_i} \right\rangle + \frac{2}{3\rho} \frac{\partial \overline{u_k' p'}}{\partial x_k} \delta_{ij} - \varepsilon_{ij} + \frac{2}{3} \varepsilon \delta_{ij},
\end{aligned}
\tag{7}
$$

where the terms on the first line are the production of the anisotropic Reynolds stresses and the terms on the second line are anisotropic turbulent transport and viscous transport, respectively. On the third line, the first three terms are pressure redistribution and the last two terms are the anisotropic dissipation, where ε_{ij} is the dissipation rate tensor

$$\varepsilon_{ij} = 2\nu \left\langle \frac{\partial u_i'}{\partial x_k} \frac{\partial u_j'}{\partial x_k} \right\rangle \tag{8}$$

and $\varepsilon = \tfrac{1}{2} \varepsilon_{ii}$. The transport equation for the mean strain rate tensor is given by

$$
\begin{aligned}
\frac{\overline{D} S_{ij}}{Dt} = & -\frac{1}{2} \left(\frac{\partial U_k}{\partial x_j} \frac{\partial U_i}{\partial x_k} + \frac{\partial U_k}{\partial x_i} \frac{\partial U_j}{\partial x_k} \right) - \frac{1}{\rho} \frac{\partial^2 P}{\partial x_i \partial x_j} \\
& + \nu \frac{\partial^2 S_{ij}}{\partial x_k \partial x_k} - \frac{1}{2} \left(\frac{\partial \overline{u_i' u_k'}}{\partial x_k \partial x_j} + \frac{\partial \overline{u_j' u_k'}}{\partial x_k \partial x_i} \right),
\end{aligned}
\tag{9}
$$

where the first term in parentheses can be rewritten as the sum of the inner products of the strain rate tensor with itself and the rotation rate tensor with itself, the second term is the Hessian of the pressure, the third term is viscous transport of the mean strain rate, and the last term in parentheses is turbulent transport.

The transport equations for ν_T depend on the choice of the model. There are many different choices for the eddy viscosity—in this work the k-ε and k-ω [14] formulations are explored—based on the variables chosen to represent ν_T and also whether the transport equations for these variables

are exactly derived or modeled. The k-ε and k-ω models are two of the most popular models and, as they are two-equation models, they are two of the simplest RANS closure models that are complete and appropriate to describe turbulent flows [15]. In this work, there are three different formulations for evaluating the model error budgets. The first uses DNS data to evaluate the terms in the exact transport equations for k, ε, and ω; this is a strictly *a priori* analysis. This analysis assesses the model error associated solely with the assumptions present in the Boussinesq model. The second and third methods both employ the model transport equations for k, ε, and ω and evaluate them through *a priori* and *a posteriori* analysis, respectively. As discussed further below, together, the *a priori* and *a posteriori* analyses assess the error cancellation present in the two models. The details of these three approaches are outlined in Secs. III A, III B 1, and III B 2.

A. Exact transport equations

1. The k-ε model

In the k-ε model, the eddy viscosity is defined via the turbulent kinetic energy k and the dissipation of turbulent kinetic energy ε,

$$\nu_T = C_\mu \frac{k^2}{\varepsilon}, \tag{10}$$

where C_μ is a model constant taken to be 0.09 [14]. The exact transport equations for the turbulent kinetic energy k and dissipation of turbulent kinetic energy ε are exactly derived with no assumptions, aside from incompressible flow with constant viscosity. The transport equation for the turbulent kinetic energy is given by

$$\frac{\overline{D}k}{Dt} = -\overline{u_i'u_j'}\frac{\partial U_i}{\partial x_j} - \frac{\partial}{\partial x_j}\left(\overline{u_j'k} + \frac{1}{\rho}\overline{u_j'p'} - \nu\frac{\partial k}{\partial x_j}\right) - \varepsilon, \tag{11}$$

where the first term is production, the second term in parentheses is transport via turbulence, pressure fluctuations, and viscosity, respectively, and the last term is dissipation. The transport equation for the dissipation is given by

$$\frac{\overline{D}\varepsilon}{Dt} = -2\nu\left(\overline{\frac{\partial u_i'}{\partial x_k}\frac{\partial u_j'}{\partial x_k}} + \overline{\frac{\partial u_k'}{\partial x_i}\frac{\partial u_k'}{\partial x_j}}\right)\frac{\partial U_i}{\partial x_j} - 2\nu\overline{u_k'\frac{\partial u_i'}{\partial x_j}}\frac{\partial^2 U_i}{\partial x_k \partial x_j} - 2\nu\overline{\frac{\partial u_i'}{\partial x_k}\frac{\partial u_i'}{\partial x_m}\frac{\partial u_k'}{\partial x_m}}$$
$$+ \frac{\partial}{\partial x_j}\left(\nu\frac{\partial \varepsilon}{\partial x_j} - \nu\overline{u_j'\frac{\partial u_i'}{\partial x_m}\frac{\partial u_i'}{\partial x_m}} - 2\frac{\nu}{\rho}\overline{\frac{\partial p'}{\partial x_m}\frac{\partial u_j'}{\partial x_m}}\right) - 2\nu^2\overline{\frac{\partial^2 u_i'}{\partial x_k \partial x_m}\frac{\partial^2 u_i'}{\partial x_k \partial x_m}}, \tag{12}$$

where the first line terms are production of dissipation, the first term in parentheses on the second line is transport of dissipation, and the final term is dissipation of dissipation [16].

With all of these transport equations, a transport equation for the model error is derived by substituting Eqs. (7), (9), (11), and (12) into Eq. (6). For the k-ε model with the exact transport equations for k and ε, the error transport equation is given by

$$\frac{De_{ij}}{Dt} = -e_{ik}\frac{\partial U_j}{\partial x_k} - e_{jk}\frac{\partial U_i}{\partial x_k} + 2\nu_T\frac{\partial U_i}{\partial x_k}\frac{\partial U_j}{\partial x_k} + \frac{2}{3}(e_{kl} - 2\nu_T S_{kl})\frac{\partial U_k}{\partial x_l}\delta_{ij} \tag{13a}$$

$$+ \frac{1}{\rho}\frac{\partial \nu_T}{\partial x_k}\left(\frac{\partial P}{\partial x_i}\delta_{jk} + \frac{\partial P}{\partial x_j}\delta_{ik}\right) \tag{13b}$$

$$+ \frac{\partial \nu_T}{\partial x_k}\left[\frac{\partial}{\partial x_j}\left(e_{ik} - 2\nu_T S_{ik} + \frac{2}{3}k\delta_{ik}\right) + \frac{\partial}{\partial x_i}\left(e_{jk} - 2\nu_T S_{jk} + \frac{2}{3}k\delta_{jk}\right)\right] \tag{13c}$$

$$+ \frac{\partial}{\partial x_k}\left[-\overline{u_i'u_j'u_k'} + \frac{2}{3}\overline{ku_k'}\delta_{ij} - \frac{\nu_T}{\rho}\left(\frac{\partial P}{\partial x_i}\delta_{jk} + \frac{\partial P}{\partial x_j}\delta_{ik}\right) + \nu\frac{\partial e_{ij}}{\partial x_k} - 2\nu S_{ij}\frac{\partial \nu_T}{\partial x_k}\right] \tag{13d}$$

$$- \nu_T \frac{\partial}{\partial x_j}\left(e_{ik} - 2\nu_T S_{ik} + \frac{2}{3}k\delta_{ik}\right) - \nu_T \frac{\partial}{\partial x_i}\left(e_{jk} - 2\nu_T S_{jk} + \frac{2}{3}k\delta_{jk}\right)\Bigg] \tag{13e}$$

$$- \frac{1}{\rho}\left\langle u_i'\frac{\partial p'}{\partial x_j} + u_j'\frac{\partial p'}{\partial x_i}\right\rangle + \frac{2}{3\rho}\frac{\partial \overline{u_k' p'}}{\partial x_k}\delta_{ij} - 2\nu\frac{\partial \nu_T}{\partial x_k}\frac{\partial S_{ij}}{\partial x_k} - \frac{4}{3}kS_{ij} \tag{13f}$$

$$+ \frac{4\nu_T S_{ij}}{k}\left[-(e_{kl} - 2\nu_T S_{kl})\frac{\partial U_k}{\partial x_l} - \frac{\partial}{\partial x_k}\left[\overline{ku_k'} + \frac{1}{\rho}\overline{p'u_k'} - \nu\frac{\partial k}{\partial x_k}\right] - \varepsilon\right] \tag{13g}$$

$$- \frac{2\nu\nu_T S_{ij}}{\varepsilon}\left[\frac{\partial}{\partial x_l}\left(\frac{\partial \varepsilon}{\partial x_l} - \overline{u_l'\frac{\partial u_k'}{\partial x_n}\frac{\partial u_k'}{\partial x_n}} - \frac{2}{\rho}\overline{\frac{\partial p'}{\partial x_n}\frac{\partial u_l'}{\partial x_n}}\right) - 2\nu\overline{\frac{\partial u_k'}{\partial x_m \partial x_n}\frac{\partial u_k'}{\partial x_m \partial x_n}}\right] \tag{13h}$$

$$+ \frac{4\nu\nu_T S_{ij}}{\varepsilon}\left[\left(\overline{\frac{\partial u_k'}{\partial x_m}\frac{\partial u_l'}{\partial x_m}} + \overline{\frac{\partial u_m'}{\partial x_k}\frac{\partial u_m'}{\partial x_l}}\right)\frac{\partial U_k}{\partial x_l} + \overline{u_m'\frac{\partial u_k'}{\partial x_l}}\frac{\partial^2 U_k}{\partial x_l \partial x_m} + \overline{\frac{\partial u_k'}{\partial x_m}\frac{\partial u_k'}{\partial x_n}\frac{\partial u_m'}{\partial x_n}}\right] \tag{13i}$$

$$- \varepsilon_{ij} + \frac{2}{3}\varepsilon\delta_{ij}. \tag{13j}$$

Note that all the terms in Eq. (13) can be classified as production (nonviscous source), dissipation (viscous source), redistribution (traceless), or transport (divergence of a flux). The terms in (13a)–(13c) are the production terms; (13d) and (13e) are the transport terms; (13f)–(13i) are redistribution terms; and the terms in (13j) are the dissipation terms. All terms from the transport equation for ν_T are classified as redistribution because they are multiplied by S_{ij} and as such are necessarily traceless for an incompressible turbulent flow. The right-hand side of the transport equation of k is found in (13g) and the right-hand side of the transport equation of ε is found in (13h) and (13i).

2. The k-ω model

For the k-ω model, the eddy viscosity is defined via the turbulent kinetic energy and the specific dissipation ω as

$$\nu_T = \frac{k}{\omega}, \tag{14}$$

where ω is defined by its relation to the dissipation as $\omega = \varepsilon/C_\mu k$ [14]. The exact transport equation for ω is then directly derived from its relation to ε using Eq. (12), which yields

$$\frac{\overline{D}\omega}{Dt} = \frac{1}{C_\mu k}\left[-2\nu\left(\overline{\frac{\partial u_i'}{\partial x_k}\frac{\partial u_j'}{\partial x_k}} + \overline{\frac{\partial u_k'}{\partial x_i}\frac{\partial u_k'}{\partial x_j}}\right)\frac{\partial U_i}{\partial x_j} - 2\nu\overline{u_k'\frac{\partial u_i'}{\partial x_j}}\frac{\partial^2 U_i}{\partial x_j \partial x_k} - 2\nu\overline{\frac{\partial u_i'}{\partial x_k}\frac{\partial u_i'}{\partial x_m}\frac{\partial u_k'}{\partial x_m}}\right.$$
$$\left. - 2\nu^2\overline{\frac{\partial u_i'}{\partial x_k \partial x_m}\frac{\partial u_i'}{\partial x_k \partial x_m}} + \frac{\partial}{\partial x_j}\left(\nu C_\mu k\frac{\partial \omega}{\partial x_j} + \nu C_\mu \omega\frac{\partial k}{\partial x_j} - \overline{\nu u_j'\frac{\partial u_i'}{\partial x_m}\frac{\partial u_i'}{\partial x_m}} - 2\frac{\nu}{\rho}\overline{\frac{\partial p'}{\partial x_m}\frac{\partial u_j'}{\partial x_m}}\right)\right]$$
$$- \frac{\omega}{k}\left[\frac{\partial}{\partial x_j}\left(-\overline{ku_j'} - \frac{1}{\rho}\overline{p'u_j'} + \nu\frac{\partial k}{\partial x_k}\right) - \overline{u_i'u_j'}\frac{\partial U_i}{\partial x_j} - C_\mu k\omega\right]. \tag{15}$$

It should be noted that, since the definitions of ν_T are exactly equivalent in both the k-ε and k-ω models, the model error transport equations are also exactly equal in these two formulations.

B. Model transport equations

1. A priori analysis

In the *a priori* analysis, all terms in the model error transport equation are evaluated with DNS data, regardless of whether they originate from the model or the exact physical quantity. This analysis provides insight into how well the models capture the underlying physics given the

physically correct data. The transport equations used for the modeled quantities k, ε, and ω in this formulation are given below.

The model transport equations for k, ε, and ω are constructed based on the idea that a transport equation is comprised of three main components: production, transport, and dissipation. The model transport equations for the standard k-ε model are given by

$$\frac{\overline{D}k}{Dt} = -\overline{u_i'u_j'}\frac{\partial U_i}{\partial x_j} - \varepsilon + \frac{\partial}{\partial x_j}\left[\left(\nu + \frac{\nu_T}{\sigma_k}\right)\frac{\partial k}{\partial x_j}\right], \tag{16}$$

$$\frac{\overline{D}\varepsilon}{Dt} = -C_{\varepsilon 1}\frac{\varepsilon}{k}\overline{u_i'u_j'}\frac{\partial U_i}{\partial x_j} - C_{\varepsilon 2}\frac{\varepsilon^2}{k} + \frac{\partial}{\partial x_j}\left[\left(\nu + \frac{\nu_T}{\sigma_\varepsilon}\right)\frac{\partial \varepsilon}{\partial x_j}\right], \tag{17}$$

where σ_k, $C_{\varepsilon 1}$, $C_{\varepsilon 2}$, and σ_ε are all model constants. The typical values for these constants and those used in this work are $\sigma_k = 1.0$, $C_{\varepsilon 1} = 1.44$, $C_{\varepsilon 2} = 1.92$, and $\sigma_\varepsilon = 1.3$ [14]. The definition of ν_T is the same as in Eq. (10). With the model transport equations for k and ε, the model error transport is derived by replacing the right-hand side of the exact k and ε equations in (13) [the terms in square brackets in (13g) and in (13h) and (13i), respectively] with the right-hand side of the model equations.

The model transport equations for the standard k-ω model are given by

$$\frac{\overline{D}k}{Dt} = -\overline{u_i'u_j'}\frac{\partial U_i}{\partial x_j} - \beta^* k\omega + \frac{\partial}{\partial x_j}\left[(\nu + \sigma^*\nu_T)\frac{\partial k}{\partial x_j}\right], \tag{18}$$

$$\frac{\overline{D}\omega}{Dt} = -\alpha\frac{\omega}{k}\overline{u_i'u_j'}\frac{\partial U_i}{\partial x_j} - \beta\omega^2 + \frac{\partial}{\partial x_j}\left[(\nu + \sigma\nu_T)\frac{\partial \omega}{\partial x_j}\right], \tag{19}$$

where β^*, σ^*, α, β, and σ are all model constants with standard values given by $\beta^* = 0.09$, $\sigma^* = 0.5$, $\alpha = \frac{5}{9}$, $\beta = \frac{3}{40}$, and $\sigma = 0.5$ [17]. The definition of ν_T is the same as in Eq. (14). The model error transport equation for the k-ω model is derived analogously to the k-ε model.

At this point, only the standard, uncorrected models are being considered in order to assess the error in the model of the lowest fidelity. Additionally, these model corrections are *ad hoc* and problem specific, so the lowest level of fidelity should be assessed first in order to understand the underlying physical inadequacies of the base models.

2. A posteriori analysis

In the *a posteriori* analysis, the same transport equations are used for the modeled k, ε, and ω as shown just above. However, while DNS data are still used to evaluate all of the terms that come from the transport of the true physical quantity $\frac{\overline{D}\mathcal{R}}{Dt}$, data from fully coupled RANS calculations are used to evaluate terms from the modeled quantity $\frac{\overline{D}\mathcal{M}}{Dt}$. Looking at Eq. (6), this means that all terms from $\frac{\overline{D}a_{ij}}{Dt}$ are calculated using DNS data and all terms from $2\nu_T\frac{\overline{D}S_{ij}}{Dt} + 2S_{ij}\frac{\overline{D}\nu_T}{Dt}$ are calculated using RANS data.

This *a posteriori* analysis serves two purposes. First, a comparison of the *a priori* and *a posteriori* results for the model transport equations provides an indication of how different the real and modeled k, ε, and ω are and how this influences the Reynolds stresses. Second, a comparison of the *a posteriori* results for the model transport equations and the *a priori* results for the exact transport equations provides an indication of how errors in the model transport equations for k, ε, and ω compensate for errors in the baseline Boussinesq model.

IV. RESULTS

The test case for the implied models approach is an incompressible turbulent channel flow. Direct numerical simulations at $\mathrm{Re}_\tau = 180$, 395, and 590 were calculated using NGA, which is a structured finite-difference solver [18,19], while the DNS data for $\mathrm{Re}_\tau = 1000$, 2000, and 5200 are from Lee

TABLE I. DNS parameters.

Re_τ	L_x	L_z	$N_x \times N_y \times N_z$	Δx^+	Δz^+	Δy_c^+
180	$4\pi\delta$	$\frac{4}{3}\pi\delta$	$256\times257\times256$	8.8	3.0	2.3
395	$2\pi\delta$	$\pi\delta$	$254\times513\times192$	9.7	6.5	2.6
590	$2\pi\delta$	$\pi\delta$	$384\times513\times384$	9.3	4.6	4.1

and Moser [20]. The computational details of the NGA simulations can be found in Table I. Here L_x and L_z are the domain size in the streamwise and spanwise directions, respectively, normalized by the channel half-width δ; N_x, N_y, and N_z are the number of grid points in the streamwise, wall-normal, and spanwise directions, respectively, resulting in the nondimensional uniform grid spacing Δx^+ and Δz^+ in the streamwise and spanwise directions, respectively, and the nondimensional nonuniform grid spacing Δy_c^+ in the wall-normal direction at the centerline. In all cases, the domain size is the same and with resolution comparable to or better than previous simulations of Moser *et al.* [21]. While data from Lee and Moser for the lower friction Reynolds numbers are available, the data do not contain information from the ε and ω model transport equations and so cannot be used to calculate the budgets for the shear component of the error for the model transport equations (since S_{12} is the only nonzero component of the mean strain rate tensor).

It should be noted that, since the flow is both statistically stationary and homogeneous in two directions (so zero mean velocity in the third), the right-hand side of all *exact* transport equations is exactly zero (i.e., zero Lagrangian derivatives). This includes the model error transport equation with exact equations for k, ε, and, ω. However, since the model transport equations for k, ε, and, ω are not exact, their right-hand sides do not balance to zero when evaluated using DNS data in the *a priori* analysis (so neither will the model error transport equation in these cases). This imbalance does not occur when the model transport equations are coupled back to the mean velocity in an *a posteriori* RANS calculation since the mean velocity is different and consistent with the model transport equations. This raises the possibility of fortuitous error cancellation, as alluded to above, which will be discussed subsequently in this section and assessed through the comparison of *a priori* and *a posteriori* results.
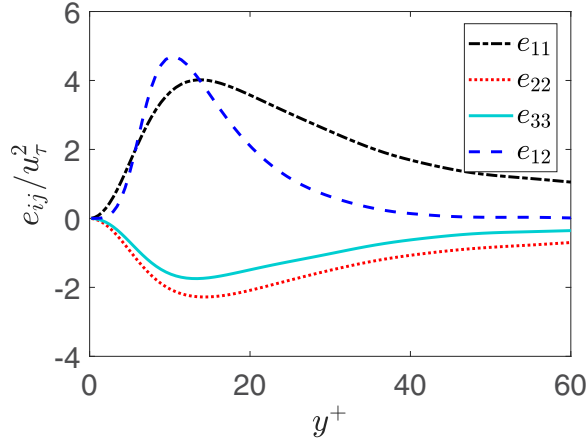
A. Channel at $Re_\tau = 180$: *A priori* analysis

The initial test case for the implied models approach is the channel at $Re_\tau = 180$. The resulting error and error budgets for the four nonzero error tensor components are shown in Fig. 1 and in Figs. 2 and 3, respectively. In the budgets, Fig. 2 shows the error production, transport, and dissipation, which are the same in all formulations, and Fig. 3 shows the model error redistribution budgets with the exact and model formulations. All of the budgets are normalized using the inner scale quantities, specifically the friction length scale δ_ν (with $y^+ = y/\delta_\nu$) and the friction velocity u_τ.

The model error shown in Fig. 1 shows that the error in all four components is confined primarily to the near-wall region. This is also clear in the model error budgets, in all three formulations, where the error in both the shear and normal components is predominantly confined to the near-wall region and the largest errors are in the shear component production and redistribution. It is possible to understand the sources of the error contributing to each component in Figs. 2(a)–2(c) by looking at the dominant terms in Eq. (13). For the different components, the dominant error production terms are given by

$$\mathcal{P}_{e_{11}} \approx -2e_{12}\frac{\partial U_1}{\partial x_2} + 2\nu_T\frac{\partial U_1}{\partial x_2}\frac{\partial U_1}{\partial x_2} + \frac{2}{3}(e_{kl} - 2\nu_T S_{kl})\frac{\partial U_k}{\partial x_\ell}, \tag{20}$$

$$\mathcal{P}_{e_{22}} \approx \frac{\partial \nu_T}{\partial x_2}\frac{\partial e_{22}}{\partial x_2} + \frac{4}{3}\frac{\partial \nu_T}{\partial x_2}\frac{\partial k}{\partial x_2} + \frac{2}{3}(e_{kl} - 2\nu_T S_{kl})\frac{\partial U_k}{\partial x_\ell}, \tag{21}$$

FIG. 1. Model error in a turbulent channel at $\mathrm{Re}_\tau = 180$.

$$\mathcal{P}_{e_{33}} \approx \frac{2}{3}(e_{kl} - 2\nu_T S_{kl})\frac{\partial U_k}{\partial x_\ell}, \tag{22}$$

$$\mathcal{P}_{e_{12}} \approx -e_{22}\frac{\partial U_1}{\partial x_2} - 2\frac{\partial \nu_T}{\partial x_2}\frac{\partial \nu_T S_{12}}{\partial x_2} + \frac{\partial \nu_T}{\partial x_2}\frac{\partial e_{12}}{\partial x_2}, \tag{23}$$

which, with the exception of the first two terms in Eq. (21) and the last two terms in Eq. (23), correspond to the misalignment of the mean strain rate tensor and the Reynolds stress tensor, which is also related to the isotropic eddy viscosity assumption. The alignment of these two tensors with a scalar coefficient is the primary assumption embedded in the Boussinesq eddy viscosity hypothesis, drawing an analogy between the Reynolds stresses and the viscous stresses. Through this analogy, it is assumed that the turbulence is in equilibrium, so a viscosity coefficient can be used to relate the mean strain rate tensor to the Reynolds stress tensor [15]. Figure 2(a) illustrates how this assumption is not applicable particularly in the near-wall region. The production error in the normal component $\mathcal{P}_{e_{22}}$ and the shear component $\mathcal{P}_{e_{12}}$ relating to the gradient of ν_T is large in the presence of inhomogeneity, such as near a wall. The equilibrium turbulence assumption implicitly assumes homogeneity, so the contribution of the gradient of the eddy viscosity to the model error is consistent with the same fundamental assumption. These misalignment errors can be alleviated by using a model that employs a nonlinear constitutive relation [22].

The error dissipation in the normal components comes from the entirety of (13j), which becomes large when the dissipation becomes anisotropic, so this represents the error in the small-scale
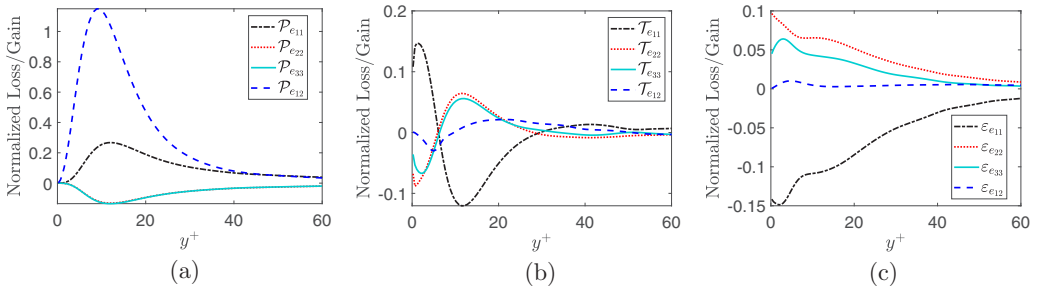
FIG. 2. Budget for e_{ij} using ν_T evaluated with the exact transport equations: (a) production, (b) transport, and (c) dissipation.
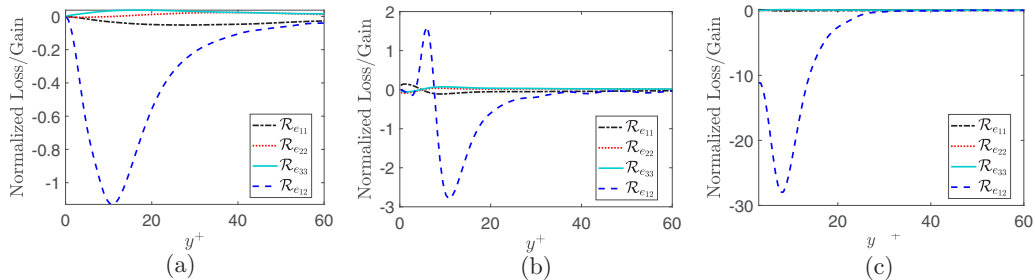
FIG. 3. Redistribution for e_{ij} with the exact and *a priori* model transport equations: (a) exact, (b) k-ε model, and (c) k-ω model.

isotropy assumption of the Boussinesq approximation. This occurs largely in the vicinity of the wall as seen in Fig. 2(c). Due to kinematic influence of the wall, the wall-normal velocity is damped much faster than the other components near the wall, resulting in the anisotropy in the dissipation tensor [23]. In this case where the k-ε and k-ω models are inadequate, the v^2-f model could be used instead as it is better suited to handle this issue of near-wall anisotropy [24]. Interestingly, at this Reynolds number, the streamwise normal component of the dissipation tensor has a considerably larger error than the spanwise normal component of the dissipation tensor, indicating the dominance of the former. This is a low-Reynolds-number effect that is revisited in Sec. IV D.

The balance to production for the shear component error is redistribution. In the exact formulation the dominant redistribution term is

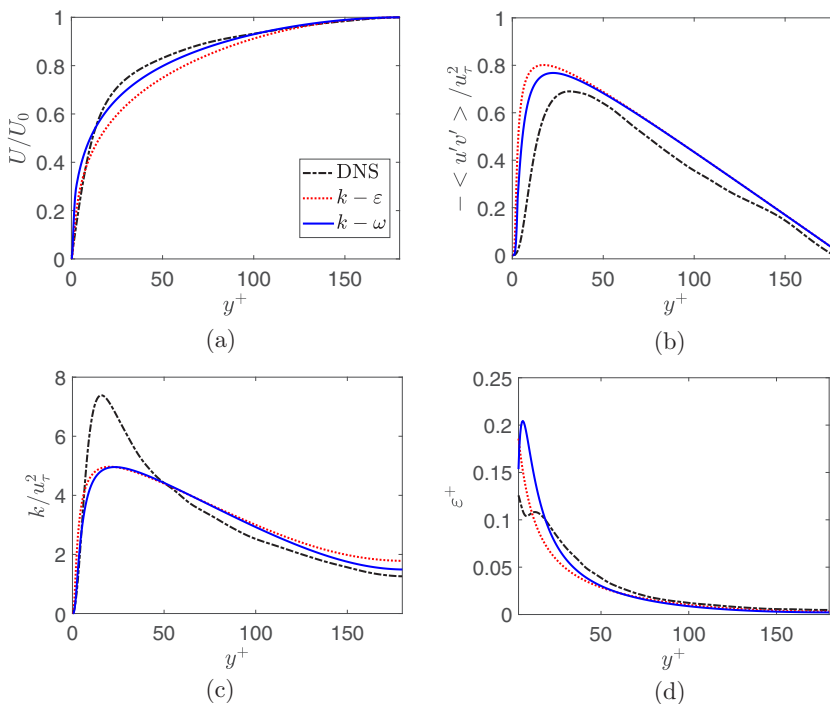$$\mathcal{R}_{e_{12}} \approx -\tfrac{4}{3} k S_{12}, \tag{24}$$

FIG. 4. Comparison of DNS with *a posteriori* k-ε and k-ω models at $\mathrm{Re}_\tau = 180$: (a) mean streamwise velocity, (b) shear stress, (c) turbulent kinetic energy, and (d) dissipation.

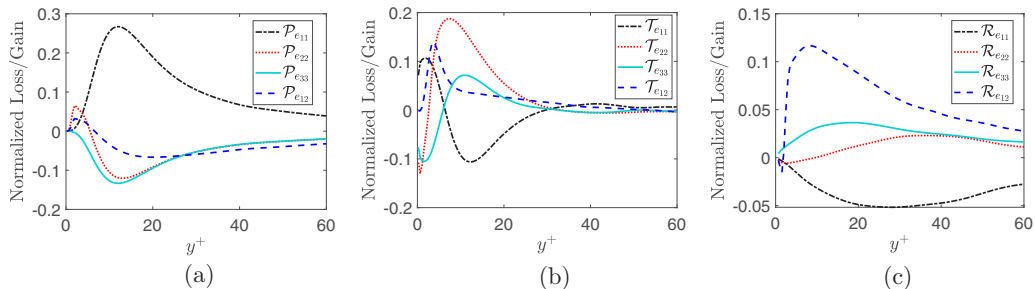FIG. 5. Error budgets for *a posteriori* k-ε analysis: (a) k-ε production, (b) k-ε transport, and (c) k-ε redistribution.

while in the model formulations the dominant terms are the right-hand sides of the k and ε or k and ω model transport equations. These errors are representative of the inadequacies of the k-ε and k-ω model transport equations and, clearly from Fig. 3, these inadequacies dominate the error of the shear component with the ω equation being grossly inadequate. However, as discussed in the next section, the inadequacies of the model equations are introduced *by design* to cancel the errors introduced by the Boussinesq hypothesis.

B. Channel at $\mathrm{Re}_\tau = 180$: *A posteriori* analysis

Figure 4 shows a comparison of the *a posteriori* predictions from the k-ε and k-ω models compared with DNS for the mean velocity, turbulent shear stress, turbulent kinetic energy, and dissipation at $\mathrm{Re}_\tau = 180$. For the most part, the k-ω model outperforms the k-ε model particularly in predicting the mean velocity profile, which is conventional knowledge for wall-bounded flows. This means that, in looking at Fig. 3, the relatively high error redistribution from the k-ω model is indicative of the fact that this model does not necessarily more accurately capture the underlying physics than the k-ε model, despite the better *a posteriori* predictions. Rather, there is more error cancellation that occurs within the k-ω model that lends itself to better predictive capabilities in wall-bounded flows. In particular, the underestimation of k [Fig. 4(c)] and overestimation of ε [Fig. 4(d)] in both the k-ε and k-ω models have been shown to provide a more accurate value for ν_T, for example, in the book from Durbin and Pettersson Reif [24]. Thus, the k-ω model provides a more accurate estimation of the mean velocity and turbulent shear stress despite being fundamentally *less* correct.

A posteriori budget analysis provides further insight into the nature of this error cancellation. As mentioned in Sec. III B 2, all terms that come from $\frac{\overline{D} 2 \nu_T S_{ij}}{Dt}$ in Eq. (6) are evaluated using data
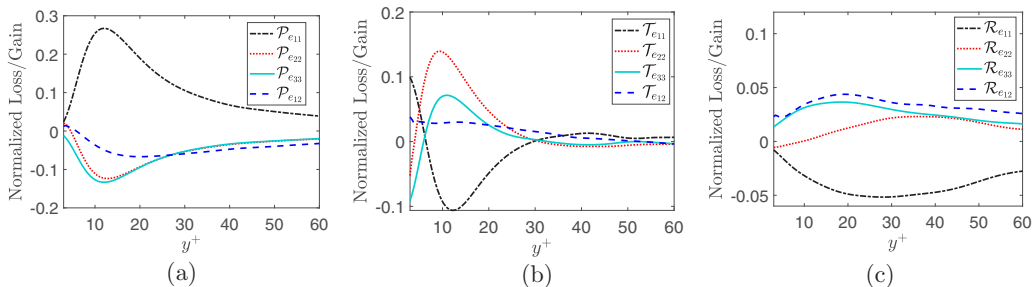

FIG. 6. Error budgets for *a posteriori* k-ω analysis: (a) k-ω production, (b) k-ω transport, and (c) k-ω redistribution.
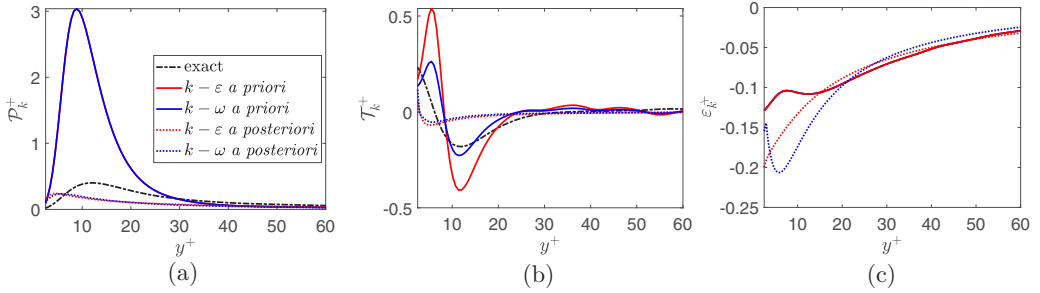
FIG. 7. Exact and model turbulent kinetic energy budgets: (a) model k production, (b) model k transport, and (c) model k dissipation.

from RANS calculations with either the k-ε or k-ω models. Figures 5 and 6 show the results of this analysis, where the production, transport, and redistribution terms from the error budgets are shown. The dissipation terms are not shown because they are unchanged from the *a priori* analysis: The nonzero contribution to the dissipation terms comes only from the physical anisotropic dissipation with the Boussinesq model itself assuming isotropic dissipation.

Comparing the results shown in Figs. 5 and 6 to those in Figs. 2 and 3, there are a few key differences. In production, the shear component, which is dominant in the *a priori* results, is not dominant in the *a posteriori* results. In contrast, the streamwise component has the largest production magnitude; however, in general, all three normal components are of the same order of magnitude. An additional point of interest is found in the redistribution terms. In the *a priori* analysis, both the k-ε and k-ω models saw increased magnitude of the shear component of the redistribution term as compared to the exact formulation with the k-ω model increasing by an order of magnitude. In the *a posteriori* analysis, there is no such increase and the shear component of the redistribution is actually larger for the k-ε model than the k-ω model. This supports the conclusion that the k-ω model provides more accurate results over the k-ε model due to error cancellation (between the Boussinesq model and the model transport equations) and not because it is more physically accurate.

C. Channel at $\mathrm{Re}_\tau = 180$: k, ε, and ω budgets

The budgets of the models equations for k, ε, and ω provide additional insight into the role of error cancellation. This was carried out through both *a priori* and *a posteriori* analysis and compared with the evaluation of the exact budgets. This analysis illustrates how well or not the
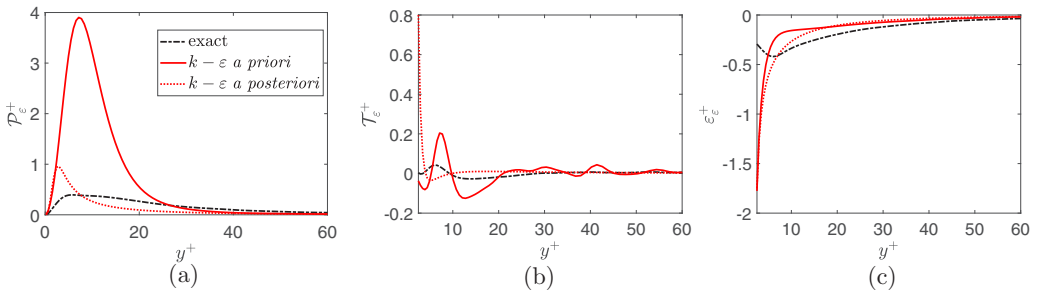

FIG. 8. Exact and model dissipation budgets: (a) model ε production, (b) model ε transport, and (c) model ε dissipation.
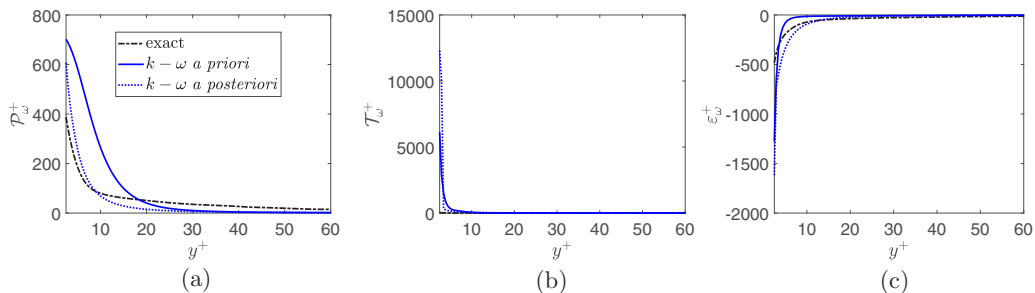
FIG. 9. Exact and model specific dissipation budgets: (a) model ω production, (b) model ω transport, and (c) model ω dissipation.

underlying physics is captured by Eqs. (16)–(19). These budget comparisons are shown in Figs. 7–9. In first looking at the turbulent kinetic energy exact and model budgets, the dissipation of turbulent kinetic energy is obviously exactly matched in the exact and *a priori* evaluation, while the *a posteriori* dissipation in both models diverges from the exact dissipation in the near-wall region. The production in the two models is the same (since the eddy viscosity is the same), though the *a priori* analysis is not a good approximation for the exact k production and the *a posteriori* analysis does not capture the correct location of the peak. In general, the *a posteriori* and *a priori* budgets are not the same and do not match the exact budgets. However, this is due to the fact that the modeled quantities k, ε, and ω from model transport equations are tuned to cancel the error in the Boussinesq model and not to faithfully represent their physical counterparts.

The exact and model comparisons of the ε and ω budgets have generally less agreement than the k budgets, which is to be expected as these model transport equations are meant to be very general characterizations of complicated differential equations involving unknown double and triple correlations [14]. As such, it is not surprising that the model budgets evaluated with the DNS data do not capture the behavior of the exact budgets, particularly in the near-wall region, but do mimic some qualitative features. Overall, the models themselves are consistently poor such that the values of k, ε, and ω are either underestimated or overestimated to provide more accurately approximated values of the eddy viscosity, mean velocity, and turbulent shear stress. Altogether, Figs. 3–9 illustrate that, while the error redistribution is largest for the k-ω model in the *a priori* analysis with the model transport equations, the error cancellation that occurs within this model, as evidenced specifically by the *a posteriori* analysis shown in Fig. 6, serves to better approximate wall-bounded flow characteristics compared with the k-ε model.

D. Extension to higher Re$_\tau$

The error budgets in the exact formulation for all four nonzero components of the error tensor were calculated at five additional friction Reynolds numbers Re$_\tau$ = 395, 590, 1000, 2000, and 5200, where the data for Re$_\tau$ = 1000, 2000, and 5200 comes from Lee and Moser [20].

Figure 10 shows the maximum (magnitude) in the error production, redistribution, and dissipation as a function of friction Reynolds number. As the Reynolds number increases, the qualitative characteristics of the error budgets do not change. Looking first at the shear component of the production and redistribution of the error, these errors are increasing in magnitude most strongly with friction Reynolds number. However, the rate of this increase is slowing with increasing Reynolds number, indicating that, if Re$_\tau$ continued to increase, the errors would plateau. This plateau in the error budgets can be seen more clearly in the normal component budgets. This behavior stems from the decrease in the anisotropy in the turbulence between the streamwise and spanwise components near the wall as the Reynolds number becomes large, which can be seen in Fig. 11. With increasingly isotropic turbulence, the use of scalar quantities to describe the state
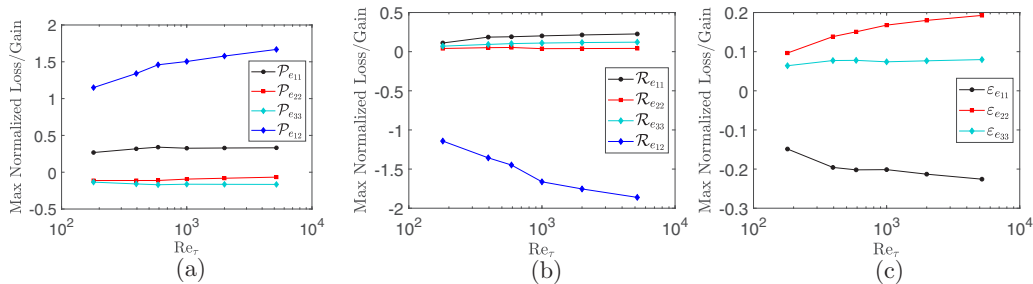
FIG. 10. Maximum (magnitude) in the error (a) production, (b) redistribution, and (c) dissipation for the error budgets with the exact ν_T transport equations.

of the flow becomes more appropriate [24]. Interestingly, given this discussion, one would expect the production and redistribution of the error to decrease in magnitude, rather than increase, with increasing Reynolds number. This then indicates some degree of error cancellation between the main assumptions (alignment of Reynolds stress with mean strain rate and the use of scalar quantities for the eddy viscosity).

Conversely, the dissipation of the error in Fig. 8(c) does not exhibit the same degree of saturation with increasing Reynolds number. As mentioned previously, due to kinematic wall blocking, the wall-normal velocity component is preferentially damped near the wall. Therefore, the wall-normal normal component of the dissipation rate tensor is essentially zero, so the dissipation can *never* be isotropic as assumed in the eddy viscosity model and the wall-normal normal component of the dissipation tensor will always be overpredicted with an isotropic assumption. Instead, near the wall, the turbulence tends toward a two-component, two-dimensional limit as the Reynolds number is increased [25]. However, at the Reynolds numbers considered here, the turbulence near the wall is more one component [25], which is the why the streamwise component of the dissipation of the error is larger than the spanwise component. As the Reynolds number is increased further, the streamwise and spanwise normal components would eventually become comparable. Note also that the scalar dissipation increases with increasing Reynolds number [25], so the magnitude of the dissipation of the error increases with increasing Reynolds number.

Taken together, these results indicate two interesting features of two-equation turbulence models. First, even if the models implicitly assume a high Reynolds number, compensating errors can
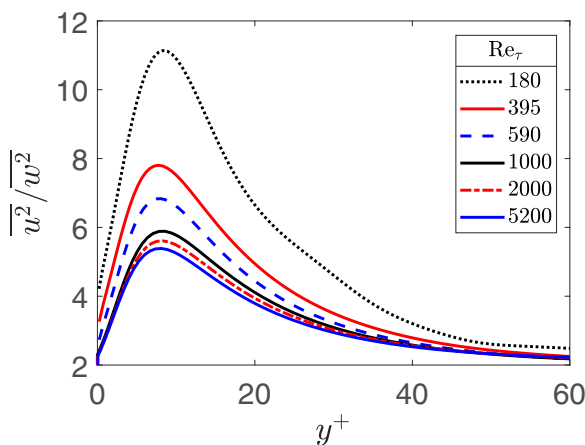

FIG. 11. Anisotropy in the turbulence with increasing Re_τ.

actually lead to lower errors at lower Reynolds number. Second, since the dissipation at the wall can never be isotropic, two-equation turbulence models relying on an isotropic dissipation can only be accurate by taking advantage of error cancellation, irrespective of Reynolds number.

E. Discussion

Both the sources of error and the error cancellation found in the k-ε and k-ω models in this work are specific to turbulent channel flow. It is expected that fundamentally different flow configurations, both canonical and otherwise, would have different sources of model error. For example, in a free shear flow the influence of anisotropy in the dissipation is not expected to greatly contribute to the error due to the general lack of small-scale anisotropic features in such flows. More complex geometries that exhibit even more complicated turbulent flow physics, such as flows with separation, would provide an interesting test case as these flows would likely uncover further sources of error and potential mechanisms of error cancellation. The implied models approach provides a quantitative framework to assess these model error sources.

In this work, the standard, uncorrected k-ε and k-ω models were analyzed using the implied models approach. The assumptions in these models are known to break down in the vicinity of walls, in which case wall functions can be employed or other models, such as v^2-f or nonlinear constituent relation models, that do not have the same shortcomings. An exploration of these more complex models in canonical wall-bounded flows, as well as other canonical and noncanonical flows, would reveal other sources of model error, which is ultimately the utility of the implied models approach. This method allows for an investigation of the reasons for model inadequacies, which has the potential to aid in the development of more accurate models.

V. CONCLUSION

In this paper, a physics-based approach for assessing model form uncertainty has been developed, which provides information regarding the dynamics of model form error. The approach develops a model error transport equation by taking the difference between the exact transport equation for a quantity of interest and the transport equation implied by the model for the quantity. This implied models approach was applied to the modeling of the Reynolds stresses, was tested on a turbulent channel flow at various friction Reynolds numbers, and was used to quantitatively assess the individual model assumptions in the Boussinesq model and show where they are prone to failure. In general, the sources of error were the misalignment between the anisotropic Reynolds stress tensor and the mean strain tensor and the anisotropy of the dissipation tensor near the wall. All of the errors were found to be largest in the near-wall region, which was expected due to the deviation from isotropy in this region. The error budgets are qualitatively similar as the Reynolds number increases.

In analyzing the model error redistribution, the right-hand sides of the k, ε, and ω transport equations appear, and it was found that error cancellation plays an important role in the accuracy of the k-ε model and especially in the accuracy of the k-ω model, which has been shown to be more accurate in wall-bounded flows for *a posteriori* calculations. The *a priori* error budget is extremely inaccurate for the k-ω model, but this is compensated in *a posteriori* application by the resulting errors in k and ω. The error cancellation that is clearly present in these models undermines their broad applicability and brings into question the goal of turbulence model development. Should a good model be derived from valid physical assumptions and be physically sound, or should a good model simply provide good *a posteriori* predictions, even if due to fortuitous error cancellation?

ACKNOWLEDGMENTS

[1] M. Meldi, D. Lucor, and P. Sagaut, Is the Smagorinsky coefficient sensitive to uncertainty in the form of the energy spectrum? Phys. Fluids **23**, 125109 (2011).

[2] W. Edeling, P. Cinnella, R. Dwight, and H. Bijl, Bayesian estimates of parameter variability in the k-ε turbulence model, J. Comput. Phys. **258**, 73 (2014).

[3] T. A. Oliver and R. D. Moser, Bayesian uncertainty quantification applied to RANS turbulence models, J. Phys.: Conf. Ser. **318**, 042032 (2011).

[4] K. Duraisamy, Z. J. Zhang, and A. P. Singh, New approaches in turbulence and transition modeling using data-driven techniques, in *Proceedings of the 53rd AIAA Aerospace Sciences Meeting, Kissimmee, Florida, 2015* (AIAA, Reston, VA, 2015), paper 2015-1284.

[5] J. R. Holland, J. D. Baeder, and K. Duraisamy, Field inversion and machine learning with embedded neural networks: Physics-consistent neural network training, in *AIAA Aviation 2019 Forum* (AIAA, Reston, 2019).

[6] M. Emory, J. Larsson, and G. Iaccarino, Modeling of structural uncertainties in Reynolds-averaged Navier-Stokes closures, Phys. Fluids **25**, 110822 (2013).

[7] G. Iaccarino, A. A. Mishra, and S. Ghili, Eigenspace perturbations for uncertainty estimation of single-point turbulence closures, Phys. Rev. Fluids **2**, 024605 (2017).

[8] C. Gorlé, S. Zeoli, M. Emory, J. Larsson, and G. Iaccarino, Epistemic uncertainty quantification for Reynolds-averaged Navier-Stokes modeling of separated flows over streamlined surfaces, Phys. Fluids **31**, 035101 (2019).

[9] C. Gorlé and G. Iaccarino, A framework for epistemic uncertainty quantification of turbulent scalar flux models for Reynolds-averaged Navier-Stokes simulations, Phys. Fluids **25**, 055105 (2013).

[10] Z. Hao and C. Gorlé, Pressure scrambling effects and the quantification of turbulent scalar flux model uncertainties, Phys. Rev. Fluids **5**, 082501(R) (2020).

[11] J.-L. Wu, J.-X. Wang, and H. Xiao, A Bayesian calibration-prediction method for reducing model-form uncertainties with application in RANS simulations, Flow Turbul. Combust. **97**, 761 (2016).

[12] H. Xiao, J.-L. Wu, J.-X. Wang, R. Sun, and C. J. Roy, Quantifying and reducing model-form uncertainties in Reynolds-averaged Navier-Stokes simulations: A data-driven, physics-informed Bayesian approach, J. Comput. Phys. **324**, 115 (2016).

[13] K. S. Klemmer and M. E. Mueller, Hierarchical model form uncertainty quantification for turbulent combustion modeling, Combust. Flame **221**, 288 (2020).

[14] D. C. Wilcox, *Turbulence Modeling for CFD* (DCW Industries, La Cañada, 2006).

[15] C. G. Speziale, in *Simulation and Modeling of Turbulent Flows*, edited by T. B. Gatski, M. Y. Hussaini, and J. L. Lumley (Oxford University Press, New York, 1996), Chap. 5.

[16] N. N. Mansour, J. Kim, and P. Moin, Reynolds-stress and dissipation-rate budgets in a turbulent channel flow, J. Fluid Mech. **194**, 15 (1988).

[17] D. C. Wilcox, Reassessment of the scale-determining equation for advanced turbulence models, AIAA J. **26**, 1299 (1988).

[18] O. Desjardins, G. Blanquart, G. Balarac, and H. Pitsch, High order conservative finite difference scheme for variable density low Mach number turbulent flows, J. Comput. Phys. **227**, 7125 (2008).

[19] J. F. MacArt and M. E. Mueller, Semi-implicit iterative methods for low Mach number turbulent reacting flows: Operator splitting versus approximate factorization, J. Comput. Phys. **326**, 569 (2016).

[20] M. Lee and R. D. Moser, Direct numerical simulation of turbulent channel flow up to $Re_\tau \approx 5200$, J. Fluid Mech. **774**, 395 (2015).

[21] R. D. Moser, J. Kim, and N. N. Mansour, Direct numerical simulation of turbulent channel flow up to $Re_\tau = 590$, Phys. Fluids **11**, 943 (1999).

[22] C. G. Speziale, On nonlinear K-l and K-ε models of turbulence, J. Fluid Mech. **178**, 459 (1987).

[23] S. B. Pope, *Turbulent Flows* (Cambridge University Press, Cambridge, 2000).

[24] P. A. Durbin and B. A. Pettersson Reif, *Statistical Theory and Modeling for Turbulent Flows* (Wiley, New York, 2010).

[25] M. Fischer, J. Jovanović, and F. Durst, Reynolds number effects in the near-wall region of turbulent channel flows, Phys. Fluids **13**, 1755 (2001).